Accepted Manuscript

Water storage changes and climate variability within the Nile Basin between 2002-2011

J.L. Awange, E. Forootan, M. Kuhn, J. Kusche, B. Heck

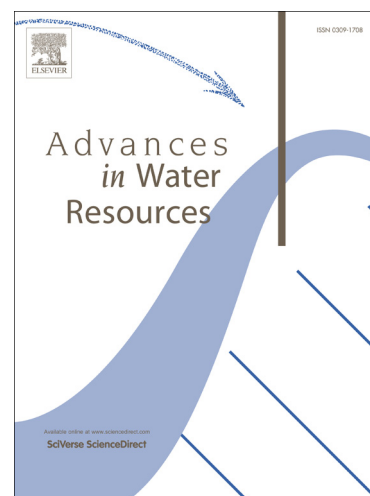# Water storage changes and climate variability within the Nile Basin between 2002-2011

J.L. Awange[a,c], E. Forootan[b,1], M. Kuhn[a], J. Kusche[b], B. Heck[c]

[a]*Western Australian Centre for Geodesy and The Institute for Geoscience Research Curtin University, Perth, Australia*
[b]*Institute of Geodesy and Geoinformation, Bonn University, Bonn, Germany*
[c]*Geodetic Institute, Karlsruhe Institute of Technology, Karlsruhe, Germany*

Abstract

Understanding water storage changes within the Nile's main sub-basins and the related impacts of climate variability is an essential step in managing its water resources. The Gravity Recovery And Climate Experiment (GRACE) satellite mission provides a unique opportunity to monitor changes in total water storage (TWS) of large river basins such as the Nile. Use of GRACE-TWS changes for monitoring the Nile is, however, difficult since stronger TWS signals over the Lake Victoria Basin (LVB) and the Red Sea obscure those from smaller sub-basins making their analysis difficult to undertake. To mitigate this problem, this study employed Independent Component Analysis (ICA) to extract statistically independent TWS patterns over the sub-basins from GRACE and the Global Land Data Assimilation System (GLDAS) model. Monthly precipitation from the Tropical Rainfall Measuring Mis-

---

Email addresses: J.Awange@curtin.edu.au (J.L. Awange),
forootan@geod.uni-bonn.de (E. Forootan), M.kuhn@curtin.edu.au (M. Kuhn),
kusche@geod.uni-bonn.de (J. Kusche), heck@gik.uni-karlsruhe.de (B. Heck)

[1]Address for corresponding author (Ehsan Forootan): Institute of Geodesy and Geoinformation, Bonn University, Nussallee 17, D53115, Bonn, NRW, Germany, Tel: 0049228736423, Fax: 0049228733029, E-mail: forootan@geod.uni-bonn.de

sion (TRMM) over the entire Nile Basin are also analysed by ICA. Such extraction enables an in-depth analysis of water storage changes within each sub-basin and provides a tool for assessing the influence of anthropogenic as well as climate variability caused by large scale ocean-atmosphere interactions such as the El Niño Southern Oscillation (ENSO) and the Indian Ocean Dipole (IOD). Our results indicate that LVB experienced effects of both anthropogenic and climate variability (i.e., a correlation of 0.56 between TWS changes and IOD at 95% confidence level) during the study period 2002-2011, with a sharp drop in rainfall between November-December 2010, the lowest during the entire study period, and coinciding with the drought that affected the Greater Horn of Africa. Ethiopian Highlands (EH) generally exhibited a declining trend in the annual rainfall over the study period, which worsened during 2007-2010, possibly contributing to the 2011 drought over GHA. A correlation of 0.56 was found between ENSO and TWS changes over EH indicating ENSO's dominant influence. TWS changes over Bar-el-Ghazal experienced mixed increase-decrease, with ENSO being the dominant climate variability in the region during the study period. A remarkable signal is noticed over the Lake Nasser region indicating the possibility of the region losing water not only through evaporation, but also possibly through over extraction from wells in the Western Plateau (Nubian aquifer).

2

1. Introduction

The Nile River Basin is one of the largest basins in the world, with an area of about 3,400,000 km² (almost one-tenth of Africa). It traverses about 6,500 km from the White Nile in the south to the Mediterranean Sea in the north as it winds its way across the boundaries of eleven countries supporting livelihoods of over 300 million people (Awange et al. , 2013a). Because of this huge size of the Nile Basin, climate variability and change that is manifested locally or regionally may have regional and even international consequences through its effects on Nile river flows (Conway , 2005).

The Nile's water resources have come under threat from both anthropogenic and natural factors (see, e.g., Hamouda et al. , 2009). Indeed, that hydrological regimes respond to climate change and anthropogenic influences have been reported, e.g., in (Beyene et al. , 2010), (Konar et al. , 2013) and (Destouni et al. , 2013). For the Nile River Basin, anthropogenic influences are attributed to increased human population that has put pressure on domestic water needs and hydroelectric power supply, all coupled with the need to sustain economic growth (e.g., Awange and Ong'ang'a , 2006; Awange et al. , 2008, 2013a,b). Furthermore, not only are the demands on water increasing, but also the available water supplies appear to be decreasing, with environmental degradation of the upper Blue Nile catchment having increased throughout the 1980s (Whittington and McClelland , 1992). For example, due to the large and increased population pressure, insufficient agricultural production, a low number of developed energy sources, and drought episodes; Ethiopia, which contributes about 85% of the Nile's annual flow (Sutcliffe and Parks , 1999), but has almost 94% of its popula-

3

26 tion depending on wood fuel, is planning major hydropower and irrigation
27 development (Block et al. , 2007; Tesemma et al. , 2010; Tesfagiorgis et al.
28 , 2011; Berhane et al. , 2013). In addition to irrigation and hydroelectric
29 power, land degradation and changes in land cover in Ethiopia where forest
30 lands are being converted to agricultural land are having impact on the Nile
31 flow (see, e.g., Senay et al. , 2009; Rientjes et al. , 2011). Such measures
32 are likely to impact on the downstream countries of Egypt and Sudan whose
33 populations have been increasing, thus posing a challenge to water alloca-
34 tion (see Whittington and McClelland , 1992; Awange and Ong'ang'a , 2006;
35 Awange et al. , 2013a,b).

36   Natural factors have been the subject of numerous studies as shown in the
37 works of Beyene et al. (2010), Conway (2005) and Yates (1998, and the ref-
38 erences therein) who investigated the influence of the changing climate on the
39 Nile waters; Ghoubachi (2010) and Sefelnasr (2007) who considered ground-
40 water movement. For the Nile river discharge, for example, the influence of
41 climate variability and change has been shown e.g., by Eltahir (1996) and
42 Amarasekera et al. (1997) to account for 25% of natural variability in annual
43 discharge. Knowledge of climate variability is essential not only for predict-
44 ing its floods and droughts (Eltahir , 1996; Korecha and Barnston , 2007),
45 but also for understanding of global atmospheric dynamics since streamflow
46 is an index of precipitation integrated over large areas (Amarasekera et al. ,
47 1997).

48   To support the management of the Nile Basin's water resources (e.g.,
49 *supply*, *demand* and *sustainable use*; Hanson et al. (2004), it is essential
50 to understand the changes in its stored water (surface, groundwater, and

4

₅₁ soil moisture) and their relation to climate variability such as the El Niño
₅₂ Southern Oscillation (ENSO) and the Indian Ocean Dipole (IOD). Due to
₅₃ its large spatial extent, however, changes in Nile Basin's stored water cannot
₅₄ be monitored using traditional methods (e.g., piezometric-based). This calls
₅₅ for satellite based methods of observation. One such satellite is the Grav-
₅₆ ity Recovery And Climate Experiment (GRACE) whose use offers a unique
₅₇ chance to monitor changes in the total water storage (TWS, i.e., an integral
₅₈ of surface, groundwater, and soil moisture storage) within the Nile Basin
₅₉ (see, e.g., Awange et al. , 2008, 2013a,b; Becker et al. , 2010; Bonsor et al.
₆₀ , 2010; Senay et al. , 2009; Swenson and Wahr , 2009; Longuevergne et al. ,
₆₁ 2012).

₆₂ The main challenges in using GRACE-TWS changes over the Nile Basin
₆₃ is that on the one hand, the derived hydrological signals are dominated by
₆₄ stronger signals, e.g., those around the lakes such as Lakes Victoria and Tana
₆₅ (see, e.g., Awange et al. , 2013b), as well as regions close to the Red Sea and
₆₆ the Mediterranean Sea (Aus der Beek et al. , 2012). Computing basin average
₆₇ water variations, therefore, is normally influenced by dominant signals such
₆₈ as that of Lake Victoria Basin (LVB), while the relatively weaker signals
₆₉ from the other regions are masked making analysis of changes in TWS over
₇₀ such sub-basins difficult. On the other hand, Rodell and Famiglietti (2001)
₇₁ pointed to the limitation of GRACE products to study basins of less than
₇₂ 200,000 km^2. Since some of the Nile's sub-basins (e.g., Lake Nasser region)
₇₃ have areas less than 200,000 km^2, thus, computing TWS changes of them is
₇₄ limited by the spatial resolution of GRACE (e.g., 400,000 km^2 in Swenson
₇₅ et al. (2003) and Tapley et al. (2004)). Previous analysis of the Nile

5

76 basin based on the GRACE satellite data have thus been unable to separate

77 the signals into their respective sub-basins for the purpose of providing an

78 in-depth analysis of spatial variations (see, e.g., Awange et al. , 2013b).

79 To overcome these challenges, in the present study; (i) we apply a higher

80 order statistical tool of Independent Component Analysis (ICA) (Spatial ICA

81 in Forootan and Kusche , 2012, 2013) over the Nile Basin (between $10°$ S to

82 $35°$ N and $25°$ E to $45°$ E) to separate GRACE-TWS changes between 2002 to

83 2011 into their spatially independent sources (i.e., sub-basins). This is then

84 followed, in (ii), by an evaluation of the impacts of global climate change on

85 the TWS within these sub-basins using global climate forcing by IOD and

86 ENSO.

87 The remainder of the study is organized as follows; in the next section, the

88 Nile Basin is briefly described. The methodology (data used in the study and

89 the analysis approaches) are outlined in Section 3, and the results discussed

90 in Section 4. Section 5 concludes the major findings.

91 **2. The Nile Basin**

92 The Nile Basin (Fig. 1) has two major tributaries, the White Nile and

93 the Blue Nile, the latter being the main source of its water. The White

94 Nile originates from the Great Lakes region of Eastern Africa, and flows

95 northwards through Uganda and South Sudan. The Blue Nile on the other

96 hand starts from Lake Tana in the Ethiopian Highlands (EH), flowing into

97 Sudan from the southeast and meets the White Nile at Khartoum in Sudan.

98 From there, the Nile passes through Egypt, which is mostly dry (i.e., 92%)

99 and Sudan, and finally discharges into the Mediterranean Sea (see, e.g., Sahin

6

₁₀₀ , 1985).

₁₀₁ The four main areas of interest to our study, whose changes in TWS could
₁₀₂ be remotely sensed using GRACE satellite data due to their larger spatial
₁₀₃ coverage (i.e., over 200,000 km^2) are (see Fig. 1): (i) Lake Victoria Basin
₁₀₄ (LVB), which is the headwaters of the White Nile; (ii) the Bahr-el-Ghazal
₁₀₅ region (BEG), the main western tributary of the Nile, and the largest sub-
₁₀₆ basin. Its supply to the Sudd wetlands is however reported by Mohamed et
₁₀₇ al. (2006) to be negligible. Nonetheless, it is included in this study to assess
₁₀₈ the impacts of climate variability on its TWS changes. The Sudd wetlands
₁₀₉ (marshes) is the region between Mongalla and Malakal, which consists of
₁₁₀ marshes and lagoons, and is believed to be where most of the White Nile's
₁₁₁ water is lost due to evaporation (Yates , 1998); (iii) the Ethiopian Highlands
₁₁₂ (EH), and the headwaters of the Blue Nile; and (iv) the Egyptian desert
₁₁₃ region consisting of Lake Nasser, where significant amounts of water are lost
₁₁₄ due to evaporation (see details of regions in Conway and Hulme , 1993). The
₁₁₅ characteristics of these regions are summarized in Table (1).

FIGURE 1

3. Data and Methodology

3.1. Data

₁₁₈ The data used in this study consisted of remotely sensed GRACE-TWS
₁₁₉ changes from 2002 to 2011, Tropical Rainfall Measuring Mission (TRMM)-
₁₂₀ derived precipitation, and water storage data from Global Land Data Assim-
₁₂₁ ilation System (GLDAS) hydrological model over the same period.

7

3.1.1. *Gravity Recovery And Climate Experiment (GRACE)*

GRACE, a joint US-German satellite project launched in March 2002, detects spatio-temporal variations of the Earth's gravity field (Tapley et al. , 2004). There are a number of institutions delivering GRACE products, each applying their own processing methodologies and, often, different background models. In this work, we examined gravity field time series provided by the German GeoForschungsZentrum (GFZ), Potsdam (Flechtner , 2007). GFZ's release (RLO4) gravity field solutions are provided at monthly resolutions and consist of a set of fully normalized spherical harmonic coefficients of the geopotential, up to degree and order 120. These coefficients are contaminated by correlated errors, manifesting as stripes in the spatial domain. These striping and high-frequency effects potentially mask hydrological signals, making their detection extremely difficult (e.g., Kusche , 2007; Awange et al. , 2009). In this regard, the GFZ solutions were smoothed using the DDK2 de-correlation filter (Kusche et al. , 2009). Filtered solutions can also be downloaded from the official website of the International Center for Global Gravity Field Models[2]. We chose RLO4 version and the DDK2 filter to be consistent with previous studies, e.g., that of Awange et al. (2013a,b). In addition, we neglected any estimates for the degree 1 coefficients due to its small contribution to water storage estimation of the basin.

In order to derive the TWS changes, residual gravity field solutions taken with respect to 9 years (assumed static) average were derived. The resulting residual geopotential coefficients were then transformed into monthly TWS

---

[2](http://icgem.gfz-potsdam.de/ICGEM/TimeSeries.html)

8

145 changes using Wahr et al. (1998)'s approach. Besides the total signals of
146 the respective sub-basins, this study explored the possibility of analyzing the
147 residual signals once the dominant signals of Lake Victoria, Lake Tana and
148 the Red Sea were removed. To remove the lakes' signals from GRACE-TWS
149 changes, we followed the approach in Swenson and Wahr (2002). The surface
150 height of each lake was assumed to be changing homogeneously. For each
151 lake, a global grid was defined by a function f, where its surface was given a
152 value 1 and 0 over the rest of the globe (i.e., equivalent to 1 mm Equivalent
153 Water Thickness (EWT) over the lake and zero over the rest of the globe).
154 The lake grid function f is then defined over a sphere (with radius R) as

$$f(\lambda, \theta) = \frac{1}{4\pi} \sum_{n=1}^{120} \sum_{m=0}^{n} \bar{P}_{nm}(\cos\theta) \, [c_{nm}^{f}\cos(m\,\lambda) + s_{nm}^{f}\sin(m\,\lambda)], \qquad (1)$$

155 where $\bar{P}_{nm}$ are the normalized associated Legendre functions, λ and θ rep-
156 resent the geocentric positional vector in spherical coordinates. Since the
157 function f was known by definition, the spectral values of c_{nm}^{f} and s_{nm}^{f}
158 in Eq. 1 were derived by integration (Wang et al. , 2006). The esti-
159 mated spherical harmonic coefficients (c_{nm}^{f} and s_{nm}^{f}) were then filtered us-
160 ing the DDK2 (Kusche et al. , 2009). Finally, each field was scaled us-
161 ing the sea surface heights (SSH) time-series (in mm) derived from Ja-
162 son 1 and 2 satellite altimetry data (Crétaux et al. , 2011). The altime-
163 try data were downloaded from the LEGOS website (http://www.legos.obs-
164 mip.fr/en/soa/hydrologie/hydroweb/). This procedure transferred SSH changes
165 of the desired lake to what GRACE could see as a whole. As an example,
166 in Fig. 2, the satellite altimetry-derived EWT changes and GRACE-TWS

9

₁₆₇ time series corresponding to Lake Victoria over the period 2002 to 2011 are

₁₆₈ shown .

FIGURE 2

₁₆₉ *3.1.2. Tropical Rainfall Measuring Mission (TRMM)*

₁₇₀   TRMM, a joint Japanese/USA satellite mission (see Kummerow et al.,

₁₇₁ 1998), launched in 1997 provides measurements of the spatial and temporal

₁₇₂ variation of the tropical rainfall in the latitude range $\pm\ 35°$ over inaccessible

₁₇₃ areas such as the oceans and unsampled terrains. TRMM data has been

₁₇₄ validated and employed in a number of studies of African precipitation, where

₁₇₅ they have been found to be adequate (see, e.g., Nicholson et al. , 2003;

₁₇₆ Awange et al. , 2013a,b). For example, Awange et al.   (2008, 2013a,b)

₁₇₇ applied TRMM to study the Nile Basin while Naumann et al. (2012) found

₁₇₈ TRMM data to be reliable enough to be used for drought monitoring over

₁₇₉ Africa. The use of TRMM satellite data for this study, therefore, is informed

₁₈₀ by the works of Awange et al.   (2013a,b) and the references therein. The

₁₈₁ present work utilized the DDK2-filtered TRMM 3B43 records for the period

₁₈₂ 2002 to May 2011 for comparisons with GRACE-TWS changes.

₁₈₃ *3.1.3. Global Land Data Assimilation System (GLDAS)*

₁₈₄   GLDAS hydrological model integrates a huge quantity of observation

₁₈₅ based data and modeling concepts (see, e.g., Rodell et al. , 2004) including a

₁₈₆ global Land Information System (LIS) at a spatial resolutions $(0.25° \times 0.25°)$

₁₈₇ (Kumar et al.   , 2006).   The monthly GLDAS data set is distributed in

₁₈₈ two parts: (i) the energy budget (EB); and (ii) the water budget (WB). To

10

189 assess the water storage variations within the Nile Basin and their compar-

190 isons with GRACE-TWS changes, we used monthly WB data (including soil

191 moisture, snow and water canopy storages) covering the period from Au-

192 gust 2002 to October 2010[2]. The GLDAS data was also filtered using the

193 same DDK2 filter used for smoothing GRACE-TWS changes to have similar

194 spectral structure.

195 *3.1.4. El Niño and Southern Oscillation (ENSO)*

196 El Niño/Southern Oscillation (ENSO) is a large scale climate variability

197 that influences the global atmospheric circulation and its impacts on regional

198 climates depend on the region and season, and the strength and spatial dis-

199 tribution of the phenomenon (Clark et al. , 2003; Colberg and Reason ,

200 2004). ENSO has a strong influence on trade winds and climate of the East

201 African region, and has been observed to weaken the Hadley circulation (Col-

202 berg and Reason , 2004). It has significant influence on rainfall over Eastern

203 Africa (Indeje et al. , 2000; Korecha and Barnston , 2007; Awange et al. ,

204 2013a,b). The warm/cold (El Niño/ La Niña) phase of ENSO is associated

205 with enhanced/depressed seasonal rainfall over various parts of the region

206 especially during the October-December (OND) rainfall season (Indeje et al.

207 , 2000; Omondi et al. , 2012, 2013a,b; Taylor et al. , 2012).

208 The Southern Oscillation (SO) is measured using Southern Oscillation

209 Index (SOI) (Hastenrath et al. , 1993). High SO phase is associated with high

210 and low pressure over the western and eastern Pacific Ocean, respectively

211 (Hastenrath et al. , 1993), resulting in enhanced westerly and cooling over the

---

[2]http:// grace.jpl.nasa.gov/data/gldas/

11

212 western parts of the ocean. The low phase has the opposite effect of enhancing

213 rainfall over the western Indian Ocean and East Africa (Hastenrath et al. ,

214 1993). The low-level circulation pattern associated with the above-normal

215 rainfall over the region is dominated by easterly inflow from the Indian Ocean

216 and westerly inflow from the Congo tropical rain forest into the positive

217 rainfall region (Anyah and Semazzi , 2006). This study used monthly SOI

218 provided by the Australian Bureau of Meteorology covering the period from

219 2002 to 2011[3].

220 *3.1.5. Indian Ocean Dipole (IOD)*

221 The Indian Ocean Dipole (IOD) and the related Indian Ocean Zonal Mode

222 (IOZM) is reflected, e.g., in the sea surface temperature (SST) data over the

223 Indian ocean. IOD has been observed to have significant influence on rainfall

224 over the East African sub-regions and other areas neighbouring the Indian

225 Ocean see, e.g., Behera et al. (2005); Black et al. (2003); Clark et al. (2003);

226 Taylor et al. (2012) and Awange et al. (2013a). IOD is caused by air-sea

227 interactions in the tropical Indian Ocean leading to the warming/cooling of

228 western/eastern tropical Indian Ocean during the positive/negative phases

229 resulting into the reversal of SST gradients and changes in the zonal wind

230 currents (Saji and Yamagata , 2003a,b).

231 The warm/cool western/eastern Indian Ocean is associated with enhanced/deficient

232 OND seasonal rainfall over the sub-region (Saji et al. , 1999; Behera et

233 al. , 2005; Black et al. , 2003; Clark et al. , 2003; Saji and Yamagata

234 , 2003a,b) resulting from the anomalous changes in Walker circulation that

---

[3](http://www.bom.gov.au/climate/enso/)

235 lead to anomalous moisture transport and convergence (Behera et al. , 2005).

236 The influence of the IOD on rainfall over the sub-region is much higher than

237 that associated with ENSO (Behera et al. , 2005), and is strongest during the

238 OND rainfall season. However, the co-occurred ENSO and IOD events are

239 stronger than those that occur independently (Saji and Yamagata , 2003a,b;

240 Song et al. , 2007; Awange et al. , 2013a). The Dipole Mode Index (DMI)

241 is the gradient of the IOD event, which is usually used as a measure of the

242 IOD influence of climate variability. In this study, we used DMI time se-

243 ries provided by the Japan Agency for Marine-Earth Science and Technology

244 (JAMSTEC) covering the period from 2002 to September 2010[4].

245 *3.2. Methodology*

246 *3.2.1. Extracting Independent Patterns*

247 At regional scale, temporal changes in total water storage (TWS), mea-

248 sured by GRACE is related to precipitation P through the water budget

249 equation

$$\frac{d(TWS(t))}{dt} = P(t) - E(t) - R(t), \qquad (2)$$

250 (Becker et al. , 2010; Rodell et al. , 2004), where P is precipitation, E for

251 evapotranspiration and R is river discharge measured in time (t). In order

252 to evaluate TWS changes obtained by GRACE, this study explores the rela-

253 tionship between GRACE-TWS changes and TRMM precipitation product

254 P over the Nile Basin. Precipitation is used here based on the fact that

---

[4](http://www.jamstec.go.jp)

13

255 previous studies have shown its capability to detect and monitor land hydro-
256 logical changes obtained from time-variable gravity observations (see, e.g.,
257 Rieser et al. , 2010; Awange et al. , 2011; Fleming et al. , 2012). When
258 comparing TRMM-rainfall with GRACE-TWS changes, however, it should
259 be kept in mind that they cannot be compared on a one-to-one basis since
260 GRACE observes the total mass changes that arises from all components of
261 the hydrological cycle, and not just precipitation. Nonetheless, precipitation
262 plays an important role in the terrestrial water balance, being the main re-
263 plenishment source of large-scale TWS changes. Analysis of the contribution
264 of E and R over the basin are outside the scope of the present study and will
265 be treated in future contributions.

266   In order to assess the water storage changes within the Nile Basin, the
267 Spatial Independent Component Analysis (Spatial ICA) approach (see, Fo-
268 rootan and Kusche , 2012; Forootan et al. , 2012) was used to extract the
269 spatially independent signals within the Nile Basin boundary, selected to ex-
270 tend from $25°\text{E} < \lambda < 45°\text{E}$ and $5°\text{S} < \varphi < 35°\text{N}$, including areas that do not
271 actually belong to the Basin, such as the Red Sea (Fig. 1). For instance,
272 assuming that time series of TWS fields, after removing their temporal mean,
273 are stored in a matrix $\mathbf{X}_{TWS} = \mathbf{X}_{TWS}(t, s)$, where t is the time, and s stands
274 for spatial coordinate (grid points). Applying Spatial ICA, $\mathbf{X}_{TWS}$ can be
275 decomposed into spatial and temporal components as

$$\mathbf{X}_{TWS} = \mathbf{A}_j \mathbf{S}_j, \tag{3}$$

276 where $\mathbf{A}_j$ $(t \times j)$ stores the j dominant unit-less temporally evolution of
277 TWS changes in its columns, and the rows of $\mathbf{S}_j$ $(j \times s)$ represent their

14

278 corresponding statistically independent spatial maps. Each temporal pattern

279 (a column of $\mathbf{A}_j$) along with its corresponding spatial pattern (a row of $\mathbf{S}_j$)

280 provides an independent mode of variability (Forootan and Kusche , 2012,

281 2013). The use of the Spatial ICA method, which is simply called ICA

282 from now on, is advantageous in two respects: first, it localizes the signals

283 and isolates those outside the basin; and second, it provides statistically

284 independent components, which enhance the interpretation of the results.

285 To understand the advantages of using ICA in localizing TWS changes

286 over the Nile Basin, let us use a simple illustration of Fig. 3 based on

287 simulated data. Let us assume that the water storage changes of the Nile

288 Basin consists of changes in lake water storage, soil moisture, and sea storage.

289 We demonstrate the power of the ICA (Forootan and Kusche , 2012) in a two-

290 step approach (see, also Forootan et al. (2012) for a simulation example on

291 Australia). In the first step, we simulate the combined lake water storage, soil

292 moisture, and sea storage over the Nile Basin and in the second step, we apply

293 the ICA approach to localize them into their respective separate components.

294 To achieve the first step, altimetry data from the LEGOS website (Crétaux

295 et al. , 2011) are used to introduce the Lake water storage changes, which

296 are then converted to EWT using the approach discussed in section 3.1.1.

297 The same approach is used to covert the level variations of the Red Sea[5]

298 into EWT changes, while the soil moisture are introduced from the GLDAS

299 model (section 3.1.3). From the first step, Fig. 3(top-A) shows the introduced

300 signals of lakes, Fig. 3(top-B) corresponds to soil moisture changes, and Fig.

---

[5](from http://coastwatch.pfeg.noaa.gov)

15

301 3(top-C) represents the introduced signals over the sea. Combined, Figs.
302 3(top-A,B, and C) leads to Fig. 3(top-D) that contains a summation of all
303 the signals. As can be seen from Fig. 3(top-D), the composition of the
304 mixed signals make it hard to interpret thereby necessitating the need for
305 ICA method to separate them and make them interpretable. Now, applying
306 the ICA method to the combined introduced patterns of Fig. (3, top-D) in
307 order to separate the signals to their respective sources, the results of Fig.
308 (3, bottom) show that the introduced water storage changes over the Red
309 Sea and Lake Nasser having been separated as the first independent mode
310 (IC1). Soil moisture pattern has been separated as the second independent
311 mode (IC2), and finally, water storage changes of Lake Vitoria are localized
312 in the third independent mode (IC3). The successful performance of ICA
313 in localizing the simulated water storage changes motivated its application
314 to real GRACE-TWS data over the Nile Basin. For more discussion on
315 the ICA-method, its performance on decomposing GRACE-derived TWS
316 fields, as well as its comparison with the second order statistical method of
317 Principal Component Analysis (PCA), we refer to Forootan and Kusche
318 (2012) and Forootan et al. (2012, 2014). The main independent patterns of
319 GRACE/GLDAS-derived TWS changes are therefore compared to those of
320 TRMM rainfall (considered as the main input of TWS changes over the Nile
321 Basin).

FIGURE 3

16

³²² *3.2.2. Correlation Analysis*

³²³ In order to study the relations between the patterns of TWS changes ³²⁴ within different Nile sub-basins and climate teleconnections (i.e., ENSO and ³²⁵ IOD), correlation analysis between ICs of GRACE-TWS changes and those ³²⁶ of ENSO and IOD indices was performed. To this end, first, the independent ³²⁷ components (ICs) of GRACE-TWS changes and indices were smoothed using ³²⁸ a 12-month moving average filter and interpolated to a regular monthly time ³²⁹ steps covering the period from October 2002 to May 2011. The temporal ³³⁰ filter was applied to decrease the effects of strong inter-annual variability on ³³¹ the computed correlations (see e.g., Forootan et al. , 2012; García-García ³³² et al. , 2011). The correlation analysis are then performed at 95% level of ³³³ confidence over the complete period in order to study the long-term impacts ³³⁴ of climate variability on TWS changes of the Nile's sub-basins.

³³⁵ **4. Results**

³³⁶ *4.1. Comparisons of GRACE-TWS, GLDAS-TWS, and TRMM-Rainfall Changes*

³³⁷ Before undertaking a detailed analysis of the water storage changes within ³³⁸ each sub-basin, overall comparison of the similarities and differences between ³³⁹ GRACE, TRMM, and GLADS was performed by applying correlation analy- ³⁴⁰ ses between data sets at 95% confidence level, where significant bounds based ³⁴¹ an asymptotic normal distribution with the variance of $1/(n-3)$ were set ³⁴² (Lehmann, and D'Abrera , 1998). Those correlations that were smaller than ³⁴³ the estimated bounds were set to zero. Figure 4 presents the spatial variation ³⁴⁴ of the correlations, indicating the high rainfall impact on TWS changes over ³⁴⁵ the tropical regions, Ber-el-Ghazal (BEG), and parts of Ethiopian Highlands

17

346 (EH). Lower correlations in other regions might reflect a higher influence of
347 unaccounted evaporation and runoff.

348   Implementing ICA on GRACE-TWS changes produced 4 significant spa-
349 tially independent components over the study region corresponding to 92% of
350 the cumulative total variance of TWS changes (see Fig 5). In comparison to
351 GRACE, GLDAS and TRMM data sets each produced 3 significant modes of
352 ICs, which corresponded to 86% and 91% of total variance respectively (see
353 Figs A1 and A2 in the Appendix). The variances suggest that the presented
354 independent modes extract the dominant large scale variability of TWS (par-
355 ticularly from GRACE compared to GLDAS) and rainfall changes within the
356 basin and thus are representative enough to be individually subjected to fur-
357 ther analysis and interpretations. For all the ICA results presented here,
358 the independent modes are ordered with respect to the variance they repre-
359 sent. The presented spatial maps are statistically independent with respect
360 to each other and are scaled by the standard deviation of their corresponding
361 temporal ICs to represent anomaly maps in mm, while the temporal ICs are
362 divided by their standard deviations to be unitless.

363   Figure 5 shows the first independent mode (spatial and temporal patterns
364 of IC1) of GRACE to be localized over the BEG region (dominated by an
365 annual signals), the second independent mode (IC2) is localized over the EH,
366 the third independent mode (IC3) over LVB, and finally the fourth indepen-
367 dent mode (IC4) is found to be over the Red Sea and the northern parts of
368 the basin. In comparison, the spatial pattern of Figure A1 (Appendix) of
369 GLDAS captures a similar pattern over the BEG, and the anomalies over
370 the northeast part of the LVB. It, however, shows a weaker signal over EH.

18

371 Figure A2 (Appendix) shows the ICA results of rainfall variability over the

372 basin, where the rainfall signal over LVB in the first mode (IC1) and EH in

373 the second mode (IC2). It does not show any rainfall related fluctuations

374 over the Red Sea. Given the high percentage of variability captured, i.e.,

375 92%, and its capability to capture signals from various regions, the proposed

376 use of GRACE-based TWS changes of the Nile sub-basins are adequate for

377 further analysis. The TWS from GLDAS and the TRMM-derived rainfall

378 changes will thus not be treated further.

379　　With the removal of Lake Victoria's signal using the procedure discussed

380 in section (3.2), the TWS from GRACE data did not change for BEG but

381 is concentrated more over the catchments for LVB and EH (Fig. 6). For the

382 Nasser region, the removal of the Red Sea and the Lake Nasser signal allowed

383 the possible impact of ground water extraction in the the Western Plateau

384 (Nubian aquifer; e.g., Sultan et al. , 2012) to be more visible (e.g., Fig. 7).

385 The results of correlations between TWS changes in different sub-basins and

386 the climate variability of ENSO and IOD are summarized in Table 2.

FIGURE 4

FIGURE 5

FIGURE 6

387 *4.2. Analysis of stored water and climate variability over the sub-basins*

388 *4.2.1. Bahr-el-Ghazal region (BEG)*

389　　Bahr-el-Ghazal (BEG) sub-basin consists of a number of rivers that orig-

390 inate from the Congo-Nile River divide and is made up of a large area of

19

very low slope such that nearly all the basin runoff and precipitation is evaporated or leaked into swamps (i.e., about 96% is lost), with only about 0.5 km^3 leaving the basin annually (Conway and Hulme , 1993). From the estimated GRACE-TWS patterns in Fig. (5, IC1), increased water storage for this region in the period between 2002 to 2003 at a rate of 64.4 mm/year was noticed. This could be explained by the increase in total annual rainfall between 2002-2004 (see, e.g., Fig. A2, IC3, in the Appendix). Between 2003 and 2006, GRACE-TWS changes showed a reduction at a rate of 29.2 mm/year, again, inline with the noticeable reduction in total annual rainfall from TRMM (see Fig. A2, IC3, in the Appendix). From 2006 to 2007, the stored water increased at a rate of 74.9 mm/year although the TRMM rainfall over this period does not show significant increase. This could imply reduced evaporation since the correlation between GRACE-TWS changes and the TRMM-rainfall over BEG gives a phase lag of 1-month at a maximum correlation of 0.53.

The ICA-derived TRMM-rainfall pattern in BEG region showed similarities to that of EH (Fig. A2, IC3, in the Appendix) but with higher amplitudes during 2002-2004 period. The BEG sub-basin experienced a reduction in total annual rainfall from 2003 to 2007, i.e., an increase in 2008, then a decreased between 2009 and 2010 before starting to increase again (Fig. A2, IC3, in Appendix). The drop seen in Fig. (A2, IC3, in Appendix) supports the deductions of Di Baldassarre et al. (2011) stating that the three sub-basins; Bahr-el-Ghazal, Sobat and Central Sudan within the Nile Basin recorded significant drops in annual precipitation.

For the study period 2002 to 2011, we found an insignificant correla-

₄₁₆ tion (0.18) between GRACE-TWS changes and IOD, and a strong positive

₄₁₇ correlation (0.71) between GRACE-TWS changes ENSO (Table 2). These

₄₁₈ correlations suggest that ENSO is the dominant climate variability associated

₄₁₉ with TWS changes over the BEG sub-basin.

₄₂₀ *4.2.2. The Ethiopian Highlands (EH); The Blue Nile*

₄₂₁ Analysing GRACE-TWS changes over Ethiopian Highlands (EH) (Fig.

₄₂₂ 5, IC2) showed a decline at a rate of 18.4 mm/year between 2002-2006. This

₄₂₃ decline can be explained by the temporal curve of the rainfall (Fig. A2, IC2

₄₂₄ in the Appendix), which shows a decline in annual rainfall for the period

₄₂₅ 2002 to the end of 2005. A similar decline was noted by Di Baldassarre

₄₂₆ et al. (2011) who studied the changes in land cover, rainfall, and stream

₄₂₇ flow of Gilgel Abbay catchment, the largest contributor to the inflow of Lake

₄₂₈ Tana (the source of the upper Blue Nile; e.g., Conway and Hulme (1993)),

₄₂₉ and found that changes in streamflow records for the period 2001-2005 could

₄₃₀ have been attributed to changes in land cover, and changes in the annual and

₄₃₁ seasonal distribution of rainfall. Between 2006-2007, GRACE-TWS changes

₄₃₂ showed an increase in stored water at a rate of 44.3 mm/year. This could

₄₃₃ be attributed to the more than normal rainfall during the peak season of

₄₃₄ July-August as indicated by the amplitude of TRMM rainfall for 2006-2007

₄₃₅ in Fig. A2, IC2 (in the Appendix). Jury (2011) found high peaks of the

₄₃₆ 2006-2007 in Ethiopian floods, which occurred in the periods 23-28 July 2006

₄₃₇ and 26-31 July 2007. The floods are attributed to rainfall associated with sea

₄₃₈ surface temperature anomalies over the western Indian Ocean (Jury , 2011).

₄₃₉ ENSO is reported to have a reverse effect, i.e., deficient rainfall tends

₄₄₀ to occur during ENSO summers (e.g., Eltahir , 1996; Korecha and Barn-

21

441 ston , 2007). Thus the Blue Nile sub-basin experienced drought episodes
442 during ENSO warmer phases and enhanced rains during the ENSO cooler
443 phases. Since 2006-2007 was an ENSO year in East Africa, one would ex-
444 pect less rainfall within the Blue Nile. The increase in the rainfall seen in
445 TRMM's temporal graph (Fig. A2, IC2, in the Appendix), therefore, could
446 be attributed to other factors such as the influence of IOD, given that this
447 study obtained a correlation of 0.61 between the TRMM rainfall and IOD
448 as opposed to 0.43 between TRMM and ENSO (results not shown). Indeed,
449 that IOD exerts influence over the same region is reported by Korecha and
450 Barnston (2007) to have occurred during the 1997 ENSO year. From 2007
451 to 2011 (Fig. 5, IC2), the temporal curves of GRACE indicate reductions
452 in TWS at a rate of 12.8 mm/year. This is due to a general reduction in
453 the total annual rainfall as seen from the TRMM in Fig. A2, IC2 (in the
454 Appendix).

455 EH recieves most of its rains in the period JJAS, which accounts for 50%
456 to 80% of annual rainfall totals over the region, contributing to high agricul-
457 tural productivity and major water reservoirs (e.g., Korecha and Barnston ,
458 2007). The peak of the JJAS rainfall occurs between July and August while
459 the dry season takes place between October to May (e.g., Rientjes et al. ,
460 2011). The temporal results of TRMM rainfall for EH in Fig. A2, IC2 (in
461 the Appendix) show a general decline in the total annual rainfall over the
462 study period, with the period 2007-2010 being mostly affected. This could
463 be due to the reduced amount the maximum rainfall recorded during the
464 long high rainfall (JJAS) season, and could possibly explain the cause of the
465 drought that faced the Greater Horn of Africa (GHA) over that period. Di

22

466 Baldassarre et al. (2011) points to a decreasing seasonality in some key
467 watersheds of the upper Nile in Ethiopia such as the southern Blue Nile.

468 For the Blue Nile sub-basin, Amarasekera et al. (1997) found a significant
469 negative correlation between discharge and ENSO. For TWS, likewise, the
470 positive correlations between ENSO and GRACE, i.e., (0.54 in Table 2),
471 support the fact that ENSO is the dominant climate variability. However,
472 the influence of IOD on TWS is also noticeable, i.e., 0.31 with respect to
473 GRACE. With the removal of Lake Tana's signal, there is a shift in the
474 GRACE signals (Fig. 6A) further towards the highlands.

475 The magnitude of the rate of change in stored water remains relatively the
476 same (i.e., 44.3 mm/year) for the period April 2006 to December 2007 even
477 after removing the signals of Lake Tana. For the period August 2002 to April
478 2006 and December 2007 to March 2012, the rate of decline in stored water
479 within the highland is of the same order of magnitude as before the removal
480 of Lake Tana's signal (e.g., 18.4 mm/year and 12.8 mm/year respectively).
481 This further confirms the well known fact that the contribution of the Blue
482 Nile's waters comes mainly from these highlands. This fact is supported by
483 the computed correlations to climate variability, which increases slightly for
484 IOD (0.47) but remains the same for ENSO (0.59, e.g., Table 2). The slight
485 increase in correlation with IOD following the removal of Lake Tana's signals
486 signifies that the stored water within the lake Tana dominates the entire
487 sub-basin.

488 *4.2.3. Lake Victoria Basin (LVB); The White Nile*

489 Fig. 5 (spatial and temporal patterns of the third mode, IC3) presents
490 the results of changes in water storage over LVB. From the spatial maps,

23

491 GRACE-TWS changes indicate dominant anomalies over the western part
492 of the Lake (Fig. 5, IC3). Looking at the spatial pattern of IC3 (Fig. 5)
493 together with its associated temporal pattern, the most significant drop in
494 water level within the basin occurred between October 2003 to the March
495 2006, consistent with the findings of Awange et al. (2008), Swenson and
496 Wahr (2009) and Becker et al. (2010). The rate of fall in water computed
497 for LVB within this period, for the data within our selected study area, was
498 84.5 mm/year. From March 2006 to May 2007, however, the TWS within
499 LVB increased at a rate of 145.2 mm/year due to the ENSO related rainfall
500 (i.e., Fig. A2, IC1 in the appendix indicates an increase in the amplitude
501 of rainfall between 2006-2007). Becker et al. (2010) who used the Global
502 Precipitation Climatology Project (GPCP) observed an increase in precipi-
503 tation from the end of 2005 to the beginning of 2007. For the study period,
504 the correlations between GRACE-TWS changes and IOD was 0.48 and 0.56
505 with ENSO suggesting that both IOD and ENSO influence TWS changes in
506 LVB.

507 The evidence that rainfall is influenced by the ENSO is supported by the
508 fact that a positive correlation of 0.72 is obtained between GRACE-TWS
509 changes and ENSO over the period 2007-2011 (see Table 1) consistent with
510 Becker et al. (2010) who obtained a positive correlation value of 0.8 between
511 TWS of GRACE and those of GPCP for the period 2005-2008. The period
512 between May 2007 and August 2009 saw a drop in the TWS of LVB at a
513 rate of 25.8 mm/year before it rose again at a rate of 49.8 mm/year due to
514 increased rainfall from 2009 (see IC1 of Fig. A2 in the Appendix).

515 As for the rainfall, the first independent mode (see, IC1 in Fig. A2 in

24

the appendix) indicate a reduction between 2004 and about mid 2006, which coincides with the drought that was experienced in the region (see, e.g., Becker et al. , 2010). During the period 2006-2007, there was ENSO and IOD induced increase in rainfall but the decline commenced after 2007 with the lowest level reached at the start of 2011. This was the lowest level of rainfall attained during the entire study period of 2002-2011, and was mainly due to a failed season and drought that affected the Greater Horn of Africa that started around that period (Omondi et al. , 2013a). We found that TRMM-rainfall changes supersede GRACE-TWS changes with a phase lag of 1 month with a maximum lag correlation of 0.52.

In Fig. 6B, the contribution of Lake Victoria's signal is removed as discussed in section 3.2 in order to study the residual catchment's stored water signals. With the removal of the signals, the remaining catchment's signal in Fig. 6B indicate a similar behaviour for the period 2003-2004 and 2006-2007 before the signal was removed. The dominant GRACE signals appears on the western side of the catchment in line with TRMM rainfall data (IC1 in Fig. A2 in the Appendix), indicating the rainfall to be more towards the western side of the catchment. During the long rainy season of March-April-May (MAM), the western side of Lake Victoria receives more rainfall than the eastern part thus recharging the stored water causing an increase (cf. Awange et al. , 2013a). Regarding the influence of climate variability on the catchment's stored water between 2002-2011, there is a decrease in correlations between ENSO (0.46) and GRACE-TWS changes after the removal of the Lake's signals (see Table 2). This could be attributed to the influence of climate variability on the rainfall that falls on the western side of Lake Vic-

541 toria, which provides most of the source of the stored water. In interpreting

542 the results of the removed Lake's signals, however, it should be pointed out

543 that remnant residual Lake's signals (e.g., Fig. 6B) also contribute to the

544 correlation, hence any conclusion needs to be taken with care.

545 In general, for LVB, over the study period of 2002 to 2011, and within our

546 selected boundary, the ICA analysis of GRACE-TWS changes showed that

547 the changes in LVB's TWS experienced periods of significant decrease (e.g.,

548 2002-2006) and significant increase (e.g., 2006-2007). Both anthropogenic

549 and climate variability could have played significant contributions to these

550 occurrences, i.e., with the 2003-2006 decrease hugely associated with the ex-

551 pansion of the Owen Falls dam (e.g., Awange et al. (2008) and Swenson

552 and Wahr (2009) while the 2005-2007 increase is associated with climate

553 variability (ENSO and IOD) as seen by comparing indices with the ICs of

554 GRACE-TWS changes. For the catchment's stored water, a similar deduc-

555 tion could be made, i.e., the expansion of the Owen Falls/Nalubale dam could

556 have affected not only the Lake but also its catchment.

557 In contrast to the White Nile's water discharge from LVB, where the

558 influence of ENSO climate variability has been shown to be weak (i.e., a

559 weak negative association with ENSO; Eltahir (1996) and Amarasekera et

560 al. (1997)), the influence of climate variability on TWS changes within the

561 basin is strong (see Table 2). LVB's general TWS trend showed a decline

562 even after the 2007 ENSO that saw a rise in its TWS. This general decline

563 impacts upon the entire Nile Basin as evident from the water levels of Lake

564 Nasser (e.g., as reported also in Becker et al. (2010) and Crétaux et al.

565 (2011)), which follows the pattern of Lake Victoria even though the Blue

26

566 Nile contributes most of the Nile's waters serving Egypt and Sudan.

567 *4.2.4. Lake Nasser region*

568 For this region, the ICA-derived GRACE-TWS anomalies were localized
569 to the northwest-southeast direction of the Red Sea (Fig. 5, IC4). This signal
570 could be largely attributed to the water storage changes within the Red Sea
571 and Lake Nasser and thus needs to be removed. The use of altimetry data
572 to remove the dominant GRACE signals from the Red Sea is supported by
573 a correlation of 0.71 between GRACE-TWS changes and the altimetry data
574 for the Red Sea. Altimetry observations provided by NOAA ERDDAP (the
575 Environmental Research Division's Data Access Program program)[6] over the
576 Red Sea were converted to EWT changes (see the conversion procedure in
577 section 3.1.1) and scaled by its variance to unit-variance (i.e., IC4 of GRACE,
578 c.f., Fig. 5D). Some differences in amplitude were detected (compare the
579 amplitudes of red and blue in Fig. 7C) mainly in 2004, 2005, and after
580 2008. The residual of GRACE-TWS changes minus Red Sea-EWT is shown
581 in black. Lake Nasser's altimetry are also converted into EWT time series
582 (same procedure as for the Red Sea), the results of which are shown in cyan.
583 As can be seen, after 2008, the EWT changes corresponding to Lake Nasser
584 is very similar to the residuals (the black line; Fig. 7C).

585 After the removal of the dominant signal of the Red Sea, the resulting
586 signal (c.f. Fig. 7A) indicates a decline in stored water in the Western
587 Plateau within the Nubian Aquifer covering Lake Nasser at a rate of 2.6
588 mm/year (cf. -3.5 mm/year for the period April 2002 to November 2010

---

[6]$http : //coastwatch.pfeg.noaa.gov$

27

589 in Sultan et al. (2012)). The loss of water in this region is attributed by
590 Sultan et al. (2012) to the fact that most of the water is extracted from
591 the Nubian Aquifer and used for agricultural purposes that largely occur
592 throughout the winter season, and also due to the fact that the Uweinat-
593 Aswan uplift prevents recharge of ground water flowing from the South to the
594 North. To strengthen this argument is the fact that expansions of some large
595 irrigation schemes such as East Uweinat project has seen heavy utilization of
596 groundwater. In the East Uweinat project, for example, the lands reclaimed
597 amounted to 1,200 ha in 1992 and 4,200 ha in 2003, with the target of
598 reclaiming a total of 75,000 ha by 2022, all of which will be irrigated using
599 groundwater (see, e.g., Salem and Pallas , 2002; Salem , 2007).

600   No dominant independent pattern was observed from TRMM and GLDAS
601 data over the region surrounding lake Nasser, indicating that precipitation
602 and soil moisture changes during the study period 2002-2011 was not the
603 source of the observed TWS changes (see Fig. 7A). This supports the
604 fact that the stored water within the Lake Nasser basin originates from the
605 other Nile sub-basins. Weaker negative correlations were observed between
606 GRACE and ENSO (-0.10) for the study period. During the same period,
607 the correlation between GRACE and IOD was 0.13. Without the Red sea
608 and Lake Tana's signals, correlations between IOD and ENSO on the one
609 hand and GRACE-TWS changes on the other hand were respectively 0.33
610 and 0.30, thus following closely to the LVB pattern (i.e., 0.48 and 0.46 for
611 IOD and ENSO, respectively, for the same).

FIGURE 7

28

TABLE 2

5. Conclusion

Using the ICA method (Spatial ICA in Forootan and Kusche , 2012; Forootan et al. , 2012), we were able to extract independent water storage patterns of the Nile sub-basins and relate them to climate variability over the study period 2002-2011. For the individual sub-basins, the study found that:

1. The stored water within LVB could have been influenced both by anthropogenic as well as climate variability (ENSO and IOD). The removal of the dominant Lake Victoria signal shows the western side of Lake Victoria having increased TWS, a possible consequence of the long rains of the MAM season that pounds the western side of the lake more.

2. Ethiopian Highlands (EH) experienced a general reduction in rainfall as seen from the TRMM data over the study period from 2002 to the end of 2010, with the period between 2005-2010 recording low rainfall during the long rainy season of JJAS and low total annual rainfall, a possible explanation for the 2011 drought that hit the Greater Horn of Africa (GHA). This reduction in rainfall impacts on TWS changes over the GHA as seen from GRACE outputs (see also Omondi et al. , 2013a).

3. Bar-el-Ghazal region showed a mixed increase/decrease in the stored water associated with increase/decrease in rainfall at different times of

29

634   the study period. The dominant climate variability in the region was

635   found to be ENSO.

636   4. For the Lake Nasser region, it is clear that the dominant EWT changes

637   of the Red Sea obscure the real impact of over extraction of water in

638   the Nubian aquifer region for irrigation purposes (e.g., Sultan et al. ,

639   2012). The situation is not helped much by the fact that there could

640   be insufficient recharge from the south-north flow of the groundwater

641   due to the presence of the Uweinat-Aswan uplift.

642   5. In general, for almost all the sub-basins, the dominant climate vari-

643   ability on GRACE-TWS changes was the ENSO, with the exception

644   of LVB and EH where the influence of IOD on GRACE-TWS changes

645   was noticeable.

31

References

Amarasekera, K.N., Lee, R.F., Williams, E.R., Eltahir, E.A.B. (1997). ENSO and the natural variability in the flow of tropical rivers. Journal of Hydrology, 200, 24-39, doi:10.1016/S0022-1694(96)03340-9.

Awange, J.L., Anyah R, Agola N, Forootan E, Omondi, P. (2013a). Potential impacts of climate and environmental change on the stored water of Lake Victoria Basin and economic implications. Water Resources Research, 49, 8160-8173, doi: 10.1002/2013WR014350.

Awange, J.L., Forootan, E., Fleming, K., Omondi, P., and Odhiambo, G., (2013b). Dominant patterns of water storage changes in the Nile basin, during 2003-2013. AGU books: Chapman Conference on Remote Sensing of Terrestrial Waters in Hawaii, USA, in press.

Awange, J.L., Fleming, K.M., Kuhn, M., Featherstone, W.E., Heck, B., Anjasmara, I. (2011). On the suitability of the $4° \times 4°$ GRACE mascon solutions for remote sensing Australian hydrology. Remote Sensing of Environment, 115, 864-875, doi: 10.1016/j.rse.2010.11.014.

Awange, J.L., Sharifi, M.A., Baur, O., Keller, W., Featherstone, W., Kuhn, M. (2009). GRACE hydrological monitoring of Australia: current limitations and future prospects. Journal of Spatial Science, 54 (1), 23-36, doi:10.1080/14498596.2009.9635164.

Awange, J.L., Sharifi, M.A., Ogonda, G., Wickert, J., Grafarend, E., Omulo, M. (2008). The Falling Lake Victoria Water Levels: GRACE, TRIMM and

32

683 CHAMP satellite analysis of the lake Basin. Water Resource Management

684 22, 775-796, doi:10.1007/s11269-007-9191-y.

685 Awange, J.L., Ong'ang'a, O. (2006). Lake Victoria: Ecology Resource and

686 Environment. Springer-Verlag, Berlin, 354pp.

687 Anyah, R.O., Semazzi, F.H.M. (2006). NCAR-AGCM ensemble simulations

688 of the variability of the Greater Horn of Africa climate, Special Issue,

689 Theoretical and Applied Climatology, 86, 39-62.

690 Aus der Beek, T., Menzel, L., Rietbroek, R., Fenoglio-Marc, L., Grayek,

691 S., Becker, M., Kusche, J., Stanev, E. (2012). Modeling the water re-

692 sources of the Black and Mediterranean Sea river basins and their im-

693 pact on regional mass changes. Journal of Geodynamics, 59-60, 157-167,

694 doi:10.1016/j.jog.2011.11.011.

695 Becker, M., LLovel, W., Cazenave, A., Güntner, A., Crétaux, J-F. (2010).

696 Recent hydrological behavior of the East African great lakes region in-

697 ferred from GRACE, satellite altimetry and rainfall observations. C. R.

698 Geoscience, 342, 223-233, http://dx.doi.org/10.1016/j.crte.2009.12.010.

699 Behera, S.K, Luo, J.J., Masson, S., Delecluse, P., Gualdi, S., Navarra, A.

700 (2005). Paramount Impact of the Indian Ocean Dipole on the East African

701 short Rains: ACGCM study. J. Climate, 18, 41-54.

702 Berhane, G., Kristine, M., Nawal.,A. and Kristine W., (2013). Water leak-

703 age investigation of micro-dam reservoirs in Mesozoic sedimentary se-

704 quences in Northern Ethiopia. Journal of African Earth Sciences,79:98-

705 110, http://dx.doi.org/10.1016/j.jafrearsci.2012.10.004

33

Beyene, T. Lettenmaier, D.P., Kabat, P. (2010). Hydrologic impacts of climate change on the Nile River Basin: implications of the 2007 IPCC scenarios. Climatic Change 100, 433-461, doi:10.1007/s10584-009-9693-0.

Black, E, Slingo, J., Sperber, K.R. (2003) An observational study of the relationship between excessively strong short rains in the coastal East Africa and Indian Ocean SST., Mon Wea. Rev. 131, 74-94.

Block, P.J., Strzepek, K., Rajagopalan B. (2007). Integrated management of the Blue Nile basin in Ethiopia. Hydropower and Irrigation Modeling. International Food Policy Research Institute, IFPRI Discussion Paper 00700.

Bonsor, H.C., Mansour, M.M., MacDonald, A.M., Hughes, A.G., Hipkin, R.G., Bedada, T. (2010). Interpretation of GRACE data of the Nile Basin using a groundwater recharge model. Hydrology and Earth System Sciences Discussions 7, 4501-4533, doi:10.5194/hessd-7-4501-2010.

Clark, C.O., Webster, P.J., Cole, J.E. (2003). Interdecadal variability of the relationship between the Indian Ocean zonal mode and East African coastal rainfall anomalies. J. Clim. 16, 548-554.

Colberg, F., Reason, C.J.C. (2004). South Atlantic response to El-Nino-Southern Oscillation induced climate variability in an ocean general circulation model. J. Geophys. Res., 109, C12015, 14pp

Conway, D. (2005). From headwater tributaries to international river: Observing and adapting to climate variability and change in the Nile Basin. Global Environmental Change 15, 99-114, doi:10.1016/j.gloenvcha.2005.01.003.

34

729   Conway, D., Hulme, M. (1993). Recent fluctuations in precipitation and
730   runoff over the Nile sub-basins and their impact on main Nile discharge.
731   Climatic Change 25:127-151, doi: 10.1007/BF01661202.

732   Crétaux J.F., Jelinski, W., Calmant, S., Kouraec, A., Vuglinski, V., Bergé-
733   Nguyen, M., Gennero, M.-C., Nino, F., Abarca Del Rio, R., Cazenave,
734   A., Maisongrande, P. (2011). SOLS: A lake database to monitor in the
735   Near real-time water level and storage variations from remote sensing data.
736   Advances in Space Research, 47 1497-1507, doi:10.1016/j.asr.2011.01.004.

737   Destouni, G., Jaramillo, F., Prieto, C. (2013). Hydroclimatic shifts driven by
738   human water use for food and energy production. Nature Climate Change
739   3, 213-217, doi:10.1038/nclimate1719

740   Di Baldassarre, G., Elshamy, M., van Griensven, A., Soliman, E., Kigobe,
741   M., Ndomba, P., Mutemi, J., Mutua, F., Moges, S., Xuan, J.-Q.,
742   Solomatine, D., Uhlenbrook, S. (2011). Future hydrology and climate
743   in the River Nile basin: a review. Hydrol. Sci. J. 56(2), 199-211,
744   doi:10.1080/02626667.2011.557378.

745   Eltahir, E.A.B. (1996). El Niño and the natural variability in the flow of the
746   Nile River. Water Resour. Res. 32 (1), 131-137.

747   Flechtner, F. (2007). GFZ Level-2 processing standards document for level-2
748   product release 0004, GRACE 327-743, Rev. 1.0.

749   Fleming K.M, Awange J.L., Kuhn, M., Featherstone, W.E. (2012). Evalu-
750   ating the TRMM 3B43 monthly precipitation product using gridded rain-

751 gauge data over Australia. Australian meteorological and oceanographic

752 Journal, 63, 421-426..

753 Forootan, E., Awange, J.L., Kusche, J., Heck, B., Eicker, A. (2012). In-
754 dependent patterns of water mass anomalies over Australia from satel-
755 lite data and models. Remote Sensing of Environment, 124, 427-443,
756 doi:0.1016/j.rse.2012.05.023.

757 Forootan E., Rietbroek, R., Kusche, J., Sharifi, M.A., Awange, J.L.,
758 Schmidt, M., Omondi, P., Famiglietti, J. (2014). Separation of large
759 scale water storage patterns over Iran using GRACE, altimetry and
760 hydrological data. Remote Sensing of Environment, 140, 580-595,
761 dx.doi.org/10.1016/j.rse.2013.09.025.

762 Forootan, E., Kusche, J. (2013). Separation of deterministic signals, using
763 independent component analysis (ICA). Stud. Geophys. Geod, 57, 17-26,
764 doi: 10.1007/s11200-012-0718-1.

765 Forootan, E., Kusche, J. (2012). Separation of global time-variable gravity
766 signals into maximally independent components. Journal of Geodesy, 86
767 (7), 477-497, doi:10.1007/s00190-011-0532-5.

768 García-García, D., Ummenhofer, C.C., Zlotnicki, V. (2011). Australian
769 water mass variations from GRACE data linked to Indo-Pacific cli-
770 mate variability. Remote Sensing of Environment, 115, 2175-2183,
771 doi:10.1016/j.rse.2011.04.007.

772 Ghoubachi, S.Y. (2010). Impact of Lake Nasser on the groundwater
773 of the Nubia sandstone aquifer system in Tushka area, south west-

36

774 ern desert, Egypt, Journal of King Saud University - Science, doi:
775 10.1016/j.jksus.2010.04.005.

776 Hamouda, M.A., Nour El-Din, M.N., Moursy, F.I. (2009). Vulnerability as-
777 sessment of water resources systems in the Eastern Nile Basin. Water Re-
778 sources Management 23, 2697-2725, doi:10.1007/s11269-009-9404-7.

779 Hanson R.T., Newhouse M.W., Dettinger M.D. (2004). A methodology to
780 assess relations between climatic variability and variations in hydrologic
781 time series in the southwestern United States. Journal of Hydrology 287(1-
782 4): 252-269, doi:10.1016/j.jhydrol.2003.10.006.

783 Hastenrath, S., Nicklis, A. Greishar, L. (1993). Atmospheric-hydrospheric
784 mechanisms of climate anomalies over the western equatorial Indian Ocean.
785 J. Geophys. Res, 98, 20 219-20 235

786 Indeje, M., Semazzi, F.H.M., Ogallo, L.J. (2000). ENSO signals in East
787 African rainfall seasons. Int. J. Climatology, 20, 19-46.

788 Jury, M.R. (2011). Meteorological scenario of Ethiopian floods in 2006-2007.
789 Theor. Appl. Climatol. 104:209-219, doi:10.1007/s00704-010-0337-0.

790 Konar, M., Todd, M.J., Muneepeerakul, R., Rinaldo, A., Rodriguez-Iturbe,
791 I. (2013). Hydrology as a driver of biodiversity: Controls on carrying ca-
792 pacity, niche formation, and dispersal. Advances in Water Resources, 51,
793 317-325, http://dx.doi.org/10.1016/j.advwatres.2012.02.009.

794 Korecha, D., Barnston, A. (2007). Predictability of June-September

37

795 Rainfall in Ethiopia. Monthly Weather Review 135: 628-650,
796 doi:10.1175/MWR3304.1.

797 Kumar, S.V., Peters-Lidard, C.D., Tian, Y., Houser, P.R., Geiger, J.,
798 Olden, S., Lighty, L., Eastman, J.L., Doty, B., Dirmeyer, P., Adams,
799 J., Mitchell, K., Wood, E.F., Sheffield, J. (2006). Land information sys-
800 tem: An interoperable framework for high resolution land surface mod-
801 eling, Environmental Modelling & amp; Software 21 (10), 1402-1415,
802 doi:10.1016/j.envsoft.2005.07.004.

803 Kummerow, C., Barnes, W., Kozu, T., Shiue, J. Simpson, J. (1998). The
804 Tropical Rainfall Measuring Mission (TRMM) sensor package. Journal of
805 Atmospheric and Oceanic Technology 15 (3), 809-817, doi:10.1175/1520-
806 0426(1998)015<0809:TTRMMT>2.0.CO;2.

807 Kusche, J. (2007). Approximate decorrelation and non-isotropic smoothing
808 of time-variable GRACE-type gravity field models. Journal of Geodesy, 81,
809 733-749, doi:10.1007/s00190-007-0143-3.

810 Kusche, J., Schmidt, R., Petrovic, S., Rietbroek, R. (2009). Decorrelated
811 GRACE time-variable gravity solutions by GFZ, and their validation using
812 a hydrological model. Journal of Geodesy, 83, 903-913, doi:10.1007/s00190-
813 009-0308-3.

814 Lehmann, E.L., D'Abrera, H.J.M. (1998). Nonparametrics: statistical meth-
815 ods based on ranks. rev. ed. Englewood Cliffs, NJ: Prentice-Hall, 464 pages.
816 ISBN 978-0-387-35212-1.

38

817 Longuevergne, L., Wilson, C.R., Scanlon, B.R., Crétaux J.F. (2012). GRACE
818   water storage estimates for the Middle East and other regions with sig-
819   nificant reservoir and lake storage. Hydrol. Earth Syst. Sci. Discuss., 9,
820   11131-11159, doi:10.5194/hessd-9-11131-2012.

821 Mohamed, Y.A., Savenije, H.H.G., Bastiaanssen, W.G.M., van den Hurk,
822   B.J.J.M. (2006). New lessons on the Sudd hydrology learned from remote
823   sensing and climate modeling. Hydrology and Earth System Sciences, Vol.
824   10: 507-518.

825 Naumann, G., Barbosa, P., Carro, H., Singleton, A., Vogt, J.
826   (2012). Monitoring drought conditions and their uncertainties in Africa
827   using TRMM Data. J. Appl. Meteor. Climatol., 51, 1867-1874.
828   doi:http://dx.doi.org/10.1175/JAMC-D-12-0113.1.

829 Nicholson, S., Some, B., McCollum, J., Nelkin, E., Klotter, D., Berte, Y., Di-
830   allo, B., Gaye, I., Kpabeba, G., Ndiaye, O., Noukpozounkou, J., Tanu, A.,
831   Thiam, A., Toure, A.A., Traore, A. (2003). Validation of TRMM and other
832   rainfall estimates with a high-density gauge dataset for West Africa: Part
833   II: Validation of TRMM rainfall products. Journal of Applied Meteorology
834   42(10), 1355–1368, doi:10.1175/1520–0450(2003)042<1355:VOT.

835 Omondi, P., Awange, J., Forootan, E., et al. (2013a). Changes in temperature
836   and precipitation extremes over the Greater Horn of Africa region from
837   1961 to 2010. International Journal of Climatology, doi: 10.1002/joc.3763.

838 Omondi, P., Awange, J., Ogallo, Ininda, J., Forootan, E. (2013b). The in-
839   fluence of low frequency sea surface temperature modes on delineated

39

840 decadal rainfall zones in Eastern Africa region. Advances in Water Re-

841 sources, dx.doi.org/10.1016/j.advwatres.2013.01.001.

842 Omondi, P., Awange, J., Ogallo, L.A., Okoola, R.A., Forootan, E.

843 (2012). Decadal rainfall variability modes in observed rainfall records

844 over East Africa and their relations to historical sea surface tem-

845 perature changes. Journal of Hydrology, Vol.464-465, Page 140-156,

846 dx.doi.org/10.1016/j.jhydrol.2012.07.003.

847 Rientjes, T.H.M.,Haile, A.T., Kebede, E., Mannaerts, C. M. M., Habib, E.,

848 Steenhuis, T. S. (2011). Changes in land cover, rainfall and stream flow in

849 Upper Gilgel Abbay catchment, Blue Nile basin - Ethiopia. Hydrol. Earth

850 Syst. Sci., 15, 1979-1989, doi:10.5194/hess-15-1979-2011.

851 Rieser, D., Kuhn, M., Pail, R., Anjasmara, I., Awange, J.L. (2010). Re-

852 lation between GRACE-derived surface mass variations and precipita-

853 tion over Australia. Australian Journal of Earth Science 57 (7), 887-900,

854 doi:10.1080/08120099.2010.512645.

855 Rodell, M., Famiglietti, J.S. (2001). An analysis of terrestrial water stor-

856 age variations in Illinois with implications for the gravity recovery

857 and climate experiment (GRACE). Water Resourc. Res. 37, 1327-1340,

858 doi:10.1029/2000WR900306.

859 Rodell M, Houser, P.R., Jambor, U., Gottschalck, J., Mitchell, K., Meng,

860 K., Arsenault, C.-J., Cosgrove, B., Radakovich, J., Bosilovich, M., Entin,

861 J.K., Walker, J.P., Lohmann, D., Toll, D. (2004). The Global Land Data

40

862 Assimilation System. Bulletin of the American Meteorological Society, 85
863 (3), 381-394.

864 Sahin, M. (1985). Hydrology of the Nile Basin. Developments in water Science
865 No. 21. Elsevier, New York 575 pp.

866 Saji, N.H., Goswami, B.N., Vinayachandran, P.N., Yamagata, T. (1999).
867 A dipolemode in the tropical Indian Ocean. Nature, 401, 360-363.
868 http://dx.doi.org/10.1038/43854.

869 Saji, N.H., Yamagata, T. (2003a) Possible impacts of Indian Ocean Dipole
870 Mode events on global climate. Climate Research, 25 (2), 151-169.

871 Saji, N.H., Yamagata, T. (2003b) Structure of SST and Surface Wind Vari-
872 ability during Indian Ocean Dipole Mode Events: COADS Observations.
873 J. Climate, 16 (16), 2735-2751.

874 Salem, O. M., and P. Pallas (2002), The Nubian Sandstone Aquifer System,
875 paper presented at Managing Shared Aquifer Resources in Africa, ISARM-
876 AFRICA, Tripoli, Libya, 2-4 June 2002.

877 Salem, O. M. (2007), Management of Shared Groundwater Basins in Libya,
878 African Water Journal, 1(1), 109-120.

879 Sefelnasr A.M. (2007). Development of groundwater flow model for water
880 resources management in the development areas of the western desert,
881 Egypt. Dissertation, Faculty of Natural Sciences III of the Martin Luther
882 University Halle-Wittenberg.

41

883 Senay, G.B., Asante, K., Artan, G. (2009). Water balance dynamics in the
884   Nile Basin. Hydrological Processes 23, 3675-3681, doi:10.1002/hyp.7364.

885 Song, Q., Vecchi, G.A., Rosati, A.J. (2007). Indian Ocean Variability in the
886   GFDL Coupled Climate Model. J. Climate, 20, 2895-2916

887 Sultan, M., Ahmed, M., Sturchio, N., Yan, Y.E., Milewski, A., Becker, R.,
888   Wahr, J., Becker, D., Chouinard, K. (2012). Assessment of the vulnerabil-
889   ities of the Nubian sandstone fossil aquifer, North Africa. Water Encyclo-
890   pedia, in press, Elsevier.

891 Sutcliffe, J.V., Parks, Y.P. (1999). The hydrology of the Nile, IAHS Special
892   publication No. 5. IAHS press, Institute of Hydrology: Wallingford, Oxford
893   Shine.

894 Swenson, S., Wahr, J., Milly, P. (2003). Estimated accuracies of regional
895   water storage variations inferred from the Gravity Recovery and Cli-
896   mate Experiment (GRACE). Water Resources Research, 39(8), 1223,
897   doi:10.1029/2002WR001808.

898 Swenson, S., Wahr, J. (2002). Methods for inferring regional surface-mass
899   anomalies from Gravity Recovery and Climate Experiment (GRACE) mea-
900   surements of time-variable gravity. Journal of Geophysical Research: Solid
901   Earth, 107(B9):2193.

902 Swenson, S., Wahr, J. (2009). Monitoring the water balance of Lake Vic-
903   toria, East Africa, from space. Journal of Hydrology 370(1-4), 163-176,
904   doi:10.1016/j.jhydrol.2009.03.008.

905 Tapley, B.D., Bettadpur, S., Ries, J.C., Thompson, P.F., Watkins, M. (2004).
906   GRACE measurements of mass variability in the Earth system. Science
907   305, 503-505, doi:10.1126/science.1099192.

908 Taylor., R.G., Todd, M.C., Kongola, L., Maurice, L, Nahozya, E., Sanga,
909   H., MacDonald, A.M. (2012). Evidence of the dependence of groundwater
910   resources on extreme rainfall in East Africa. Nature Climate Change 3,
911   374-378.

912 Tesemma, Z.K., Mohamed, Y.A., Steenhuis, T.S. (2010). Trends in rainfall
913   and runoff in the Blue Nile Basin: 1964-2003. Hydrol. Process. 24, 3747-
914   3758, doi:10.1002/hyp.7893.

915 Tesfagiorgis, K., Gebreyohannes, T., De Smedt, F., Moeyersons, J., Hagos,
916   M., Nyssen, J., and Deckers, J., 2011. Evaluation of groundwater resources
917   in the Geba basin, Ethiopia. Bulletin Of Engineering Geology And The
918   Environment. 70(3). p.461-466

919 Wahr, J., Molenaar, M., Bryan, F. (1998). Time variability of the Earth's
920   gravity field: Hydrological and oceanic effects and their possible detection
921   using GRACE. Journal of Geophysical Research 103 (B12), 30205-30229,
922   DOI:10.1029/98JB02844.

923 Wang, H., Wu P., Wang, Z. (2006). An approach for spherical harmonic
924   analysis of non-smooth data. Computers and Geosciences, 32 (10):1654-
925   1668.

926 Whittington, D., McClelland, E. (1992). Opportunities for regional and inter-

927   national cooperation in the Nile Basin. Water International 17(3), 144-154,

928   doi:10.1080/02508069208686134.

929   Yates, D.N., Strzepek, K.M. (1998). Modelling the Nile Basin un-

930   der climate change. Journal of Hydrologic Engineering 3(2), 98-108,

931   doi:10.1061/(ASCE)1084-0699(1998)3:2(98).

₉₃₂ **Appendix: Dominant Independent Patterns of GLDAS TWS, and**
₉₃₃ **TRMM Rainfall for the entire Nile Basin**

FIGURE A1

FIGURE A2

₉₃₄

Table 1: Characteristics of the Nile sub-basins

	Area	Catchment	Remark
Lake Victoria	258,000 km^2	Lakes Kyoga (75,000 km^2) Albert, Elbert, George (48,000 km^2)[a] Semiliki Basin	Head Waters of the While Nile
Barrel-Ghazel (BEG)	526,000 km^2	Congo-Nile River divide Large area of low slope	About 96%[b] of basin runoff and precipitation is lost to evaporation and leakage to swamp
Ethiopian Highland (EH)	300,000 km^2	Lake Tana Region (20000 km^2) Upper Blue Nile region (150,000 km^2) Lower Blue Nile region (60,000 km^2) Dinda Rahad region (60,000 km^2)	Head waters[a] of the Blue Nile contributing about 65% of the Nile waters.
Egypt Desert Region		Lake Nasser (formed by Aswan dam)	Water loss due to evaporation

[a] Yates (1998)

[b] Conway and Hulme (1993)

46

Table 2: Correlation coefficient between independent patterns of TWS derived from GRACE and climate variability of IOD (in bold) and ENSO (in normal text) over the Nile sub-basins. Correlations are computed at 95% level of confidence. The insignificant values are morked.

Basin	Correlation
Barh-El-Ghazal	+**0.18** (insignificant)
IC1 GRACE	+0.71
Ethiopian Highlands	
(with the red Sea and	+**0.31**
the lake's signals)	+0.54
IC2 GRACE	
Ethiopian Highlands	
(without the red Sea and	+**0.47**
the lake's signals)	+0.59
IC2 GRACE	
Lake Victoria Basin	
(with the red Sea and	+**0.48**
the lake's signals)	0.56
IC3 GRACE	
Lake Victoria Basin	
(without the red Sea and	+**0.48**
the lake's signals)	0.46
IC3 GRACE	
The Nasser region	
(with the red Sea and	+**0.13** (insignificant)
the lake's signals)	−0.10 (insignificant)
IC4 GRACE	
The Nasser region	
(without the red Sea and	+**0.33**
the lake's signals)	+0.30
IC4 GRACE	

Figure 1:   The Nile Basin (brown shaded region) with the major sub-basins used in the study shown.
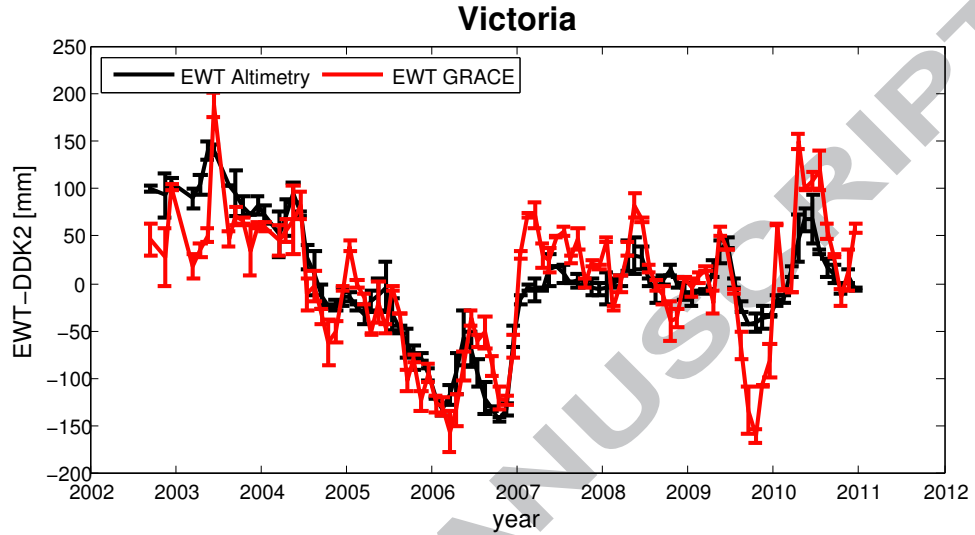
Figure 2: Satellite altimetry-derived signals for Lake Victoria (after smoothing with the DDK2 filter (Kusche et al. , 2009) and conversion to equivalent water thickness (EWT)). Both time series are centered with respect to their temporal means. The altimetry derived EWT signals represents a smoother pattern compared to the GRACE signals, which might be due to the fact that it contains only water level changes of Lake Victoria and not water storage changes over the surrounding regions of the lake. Error-bars for the GRACE-derived TWS are obtained by propagating the errors of spherical harmonics, after DDK2 filtering, to TWS without considering the covariances. Computing the error-bars for altimetry-derived TWS is done by considering the accuracy provided in LEGOS data (Crétaux et al. , 2011)

49
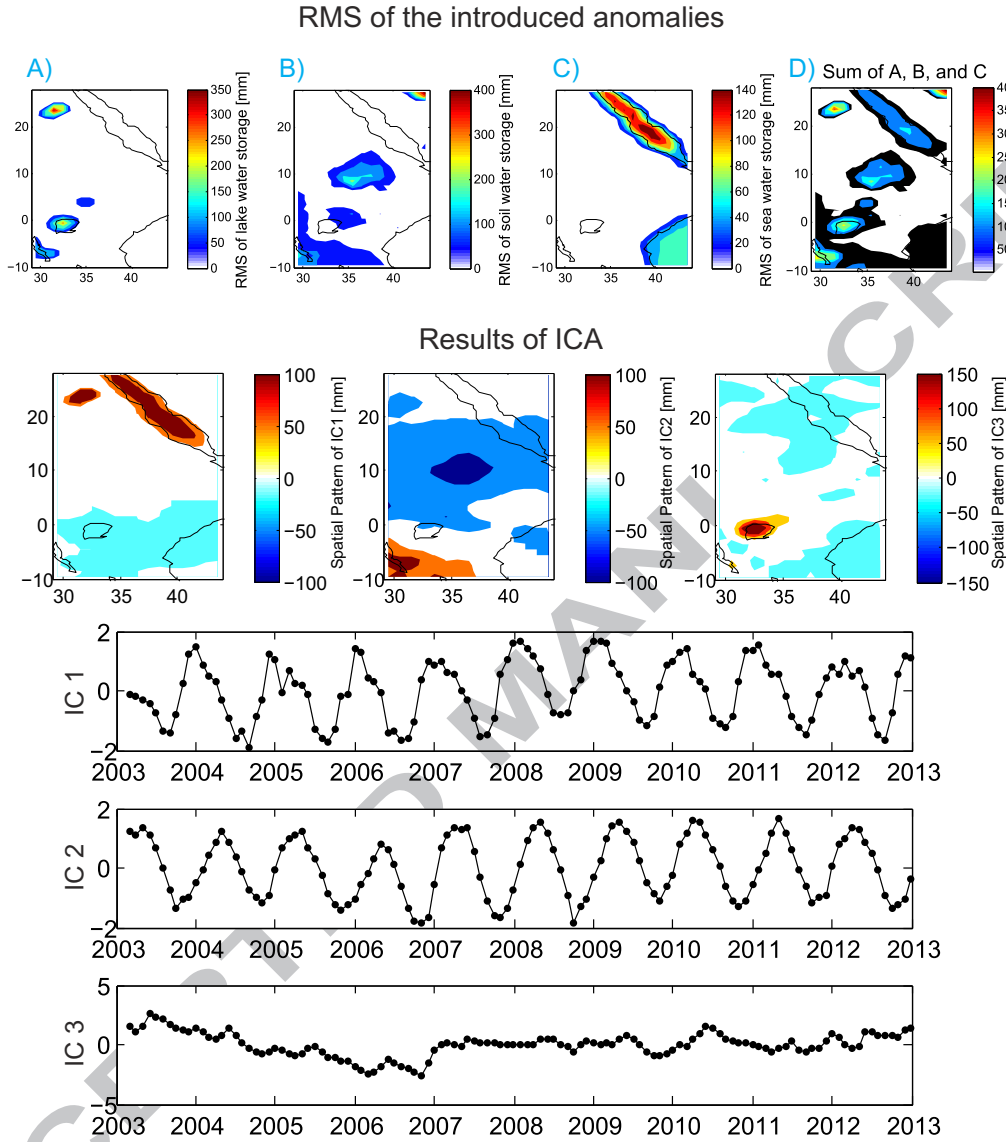
Figure 3: (top) Root mean squares of the introduced water storage changes over the major lakes of the Nile Basin, soil moisture changes of the basin and non-tidal water storage changes of the Red Sea; (Bottom) The first three independent modes, derived from ICA. The results show that the strong signal of Lake Victoria (IC3) can successfully be separated from those of the Red Sea and Lake Nasser (IC1) and those of soil moisture (IC2).
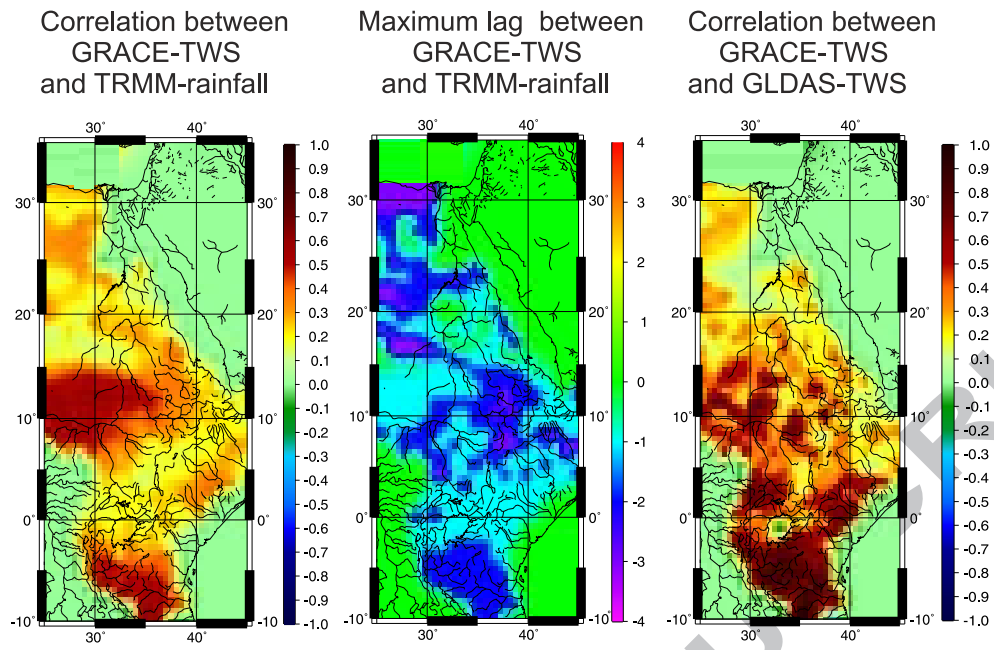
50

Correlation between
GRACE-TWS
and TRMM-rainfall

Maximum lag between
GRACE-TWS
and TRMM-rainfall

Correlation between
GRACE-TWS
and GLDAS-TWS

Figure 4: (left) Correlation between GRACE and TRMM; (center) phase lag between GRACE and TRMM in months; and (right) correlation between GRACE and GLDAS. The results show high rainfall impacts on TWS changes over the tropical regions, Bar-el-Ghazal (BEG) and parts of Ethiopian Highlands (EH)
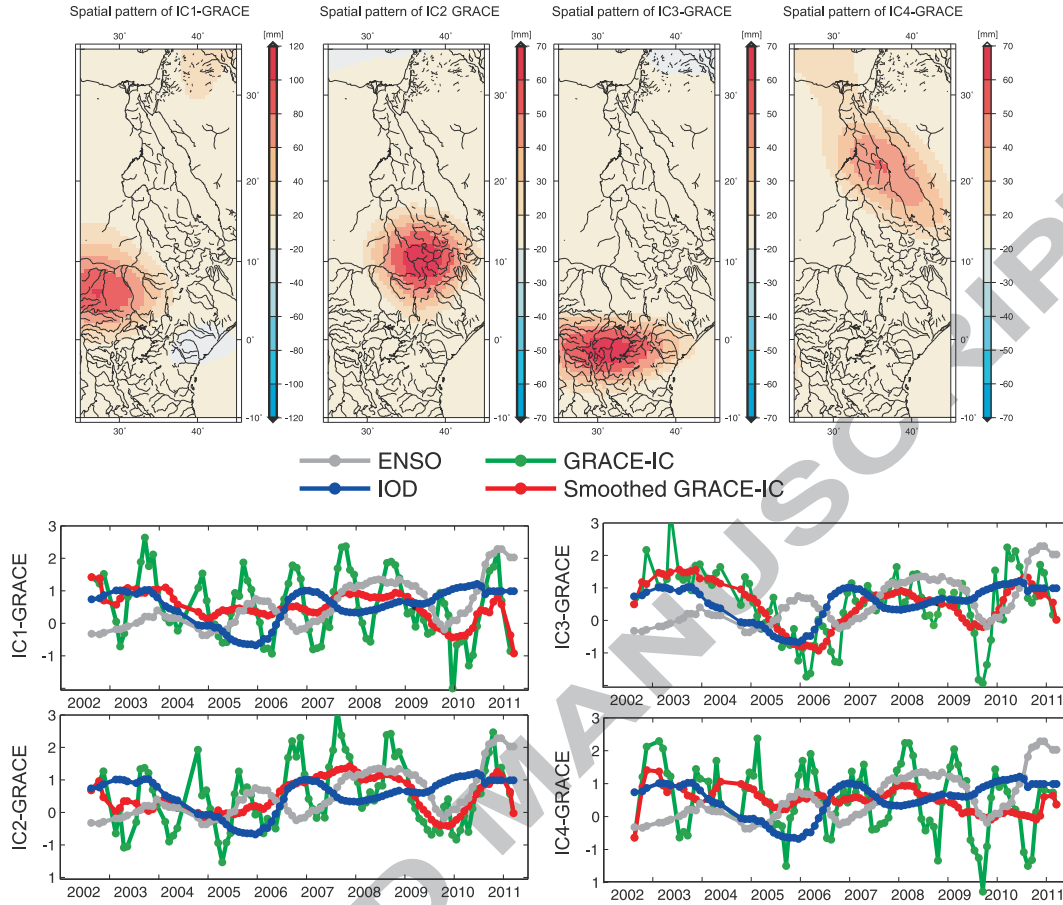
51

Figure 5: ICA decomposition of GRACE TWS signal within the Nile Basin using the proposed ICA method of Forootan and Kusche (2012, 2013). The upper panels are the spatial pattern of each IC. Note that the Nile Basin's TWS signal is separated (localized) by the ICA method into 4 significant spatially independent components (BEG (left), EH (second from left), LVB (third from left) and Red Sea (right). Together, these four signals computed over the Nile Basin account for 92% of cumulative total variance of TWS changes. In the lower panel, their corresponding time series (ICs) overlaid on smoothed time series of the loading, as well as ENSO and IOD indices.
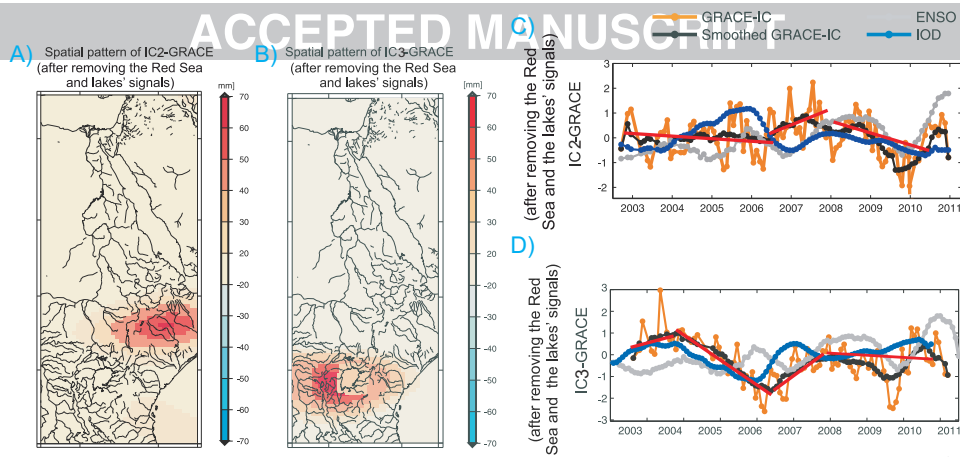
52

Figure 6: Dominant independent patterns of GRACE TWS after removing the contribution of Lakes Tana and Victoria surface water signals. Spatial patterns show the concentration of the remaining signals (after removal) over the Ethiopian Highlands (panel A) and the western part of Lake Victoria Basin (panel B). Panels C and D shows their corresponding time series (ICs) overlaid on smoothed time series of the loading and ENSO and IOD
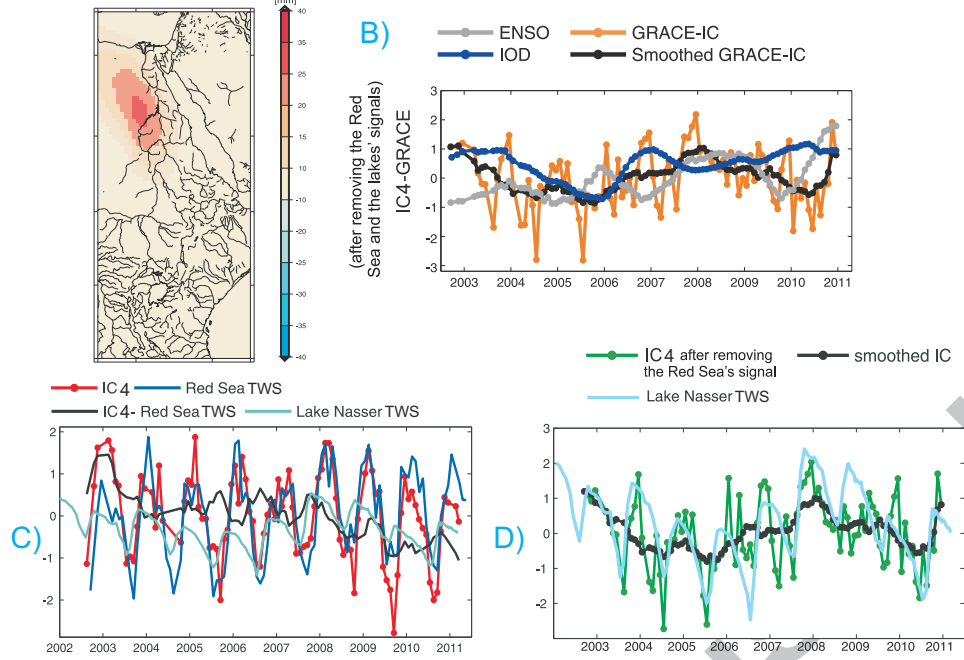
53

Figure 7: Dominant independent pattern of GRACE-TWS changes for the Nasser region. A) Spatial pattern of IC4 derived from GRACE-TWS changes after correction for the water storage changes of the Red Sea; B) the corresponding temporal evolution of (A) and its comparison with the ENSO and IOD indices; C) comparison of IC4 in (B) with the signal of the Red Sea and Lake Nasser; and D) an overview of IC4 after removing the signal of the Red Sea and its comparison with the signal of Lake Nasser. We should mention here that the Lake Nasser TWS of (C) and (D) represent the same quantity. To enhance the visual comparison, that of (D), is however, vertically shifted to the mean of IC4
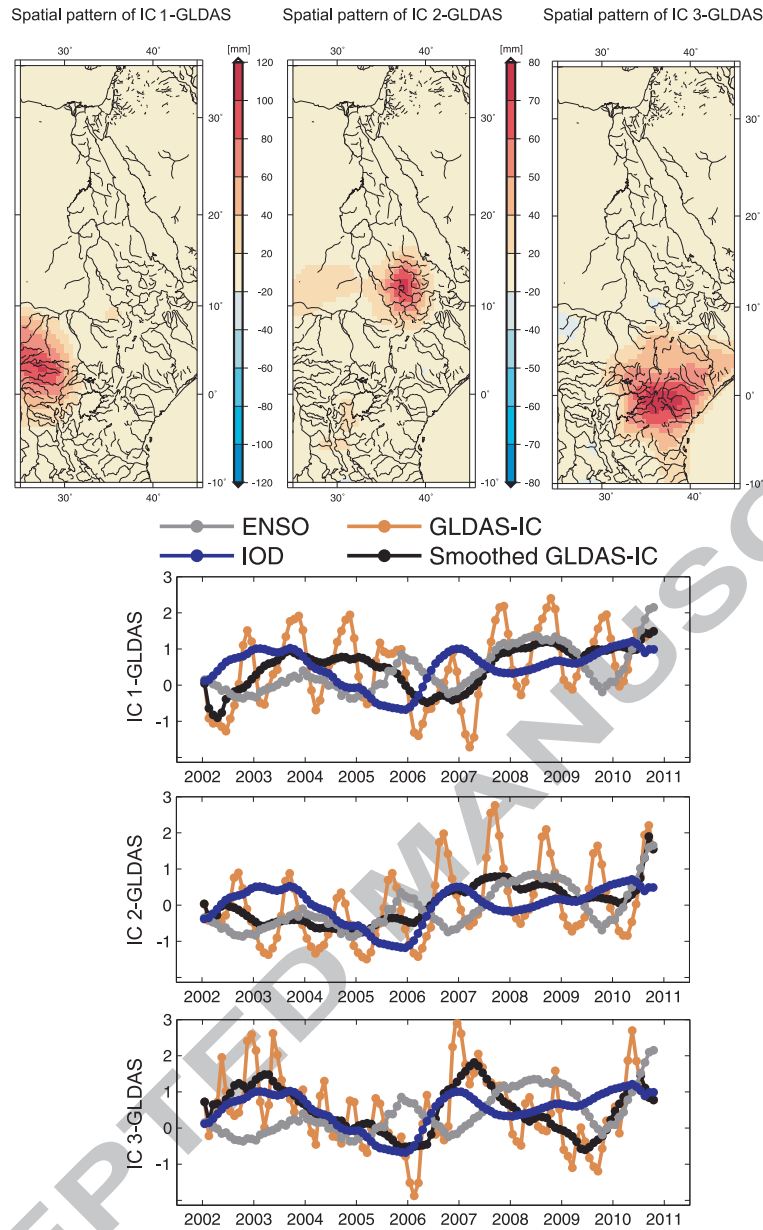
A1: ICA decomposition of GLDAS water storage data within the Nile Basin accounting for 86% of cumulative total variance of GLDAS-TWS changes. The linear rates of TWS changes corresponding to each sub-basin are also reported in the figure. IC2 and IC3 of GLDAS are comparable to those of GRACE, while IC4 of GLDAS is concentrated over the eastern part of the LVB. However, no concentration over the northern part of the basin (e.g., IC6 of GRACE) is found from GLDAS data

55
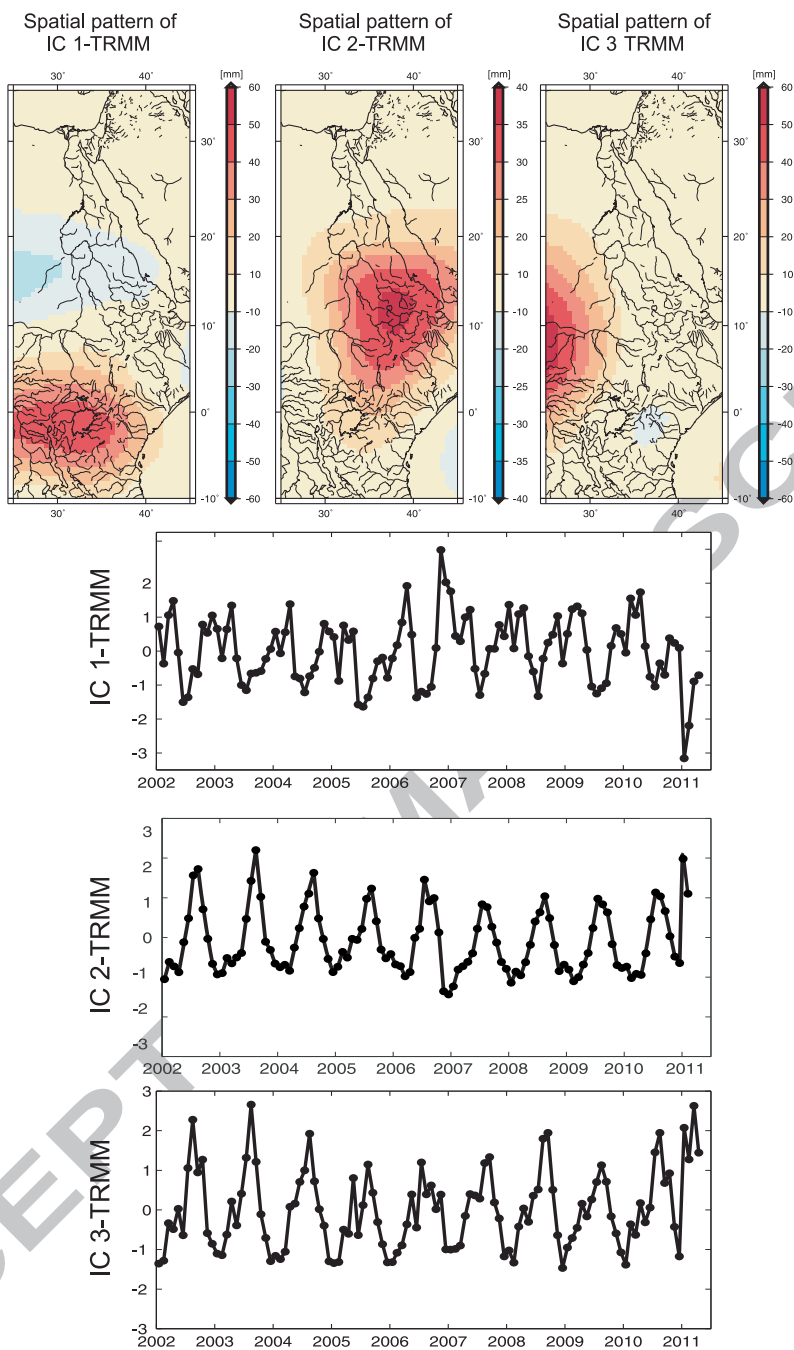
A2: ICA decomposition of TRMM derived rainfall data within the Nile Basin accounting for 91% of cumulative total variance of rainfall changes. IC3 is localized over LVB, IC4 over the EH and IC5 over the BEG region

56

Highlights

1. TWS of independent sub-basins within the Nile Basin are extracted
2. Ethiopian Highlands shows an overall declining trend in its rainfall during 2002-2011
3. Lake Nasser loses water storage through evaporation and over-extraction
4. Bar-el-Ghazal does not show a dominant multi-year change in water storage
5. ENSO was the dominant climate variability of the Nile Basin during 2002-2011